

# Multi-wavelength study of IRAS 19254-7245 – The Superantennae<sup>\*</sup>

L. Vanz<sup>1</sup>, S. Bagnulo<sup>1</sup>, E. Le Floc'h<sup>1,2</sup>, R. Maiolino<sup>3</sup>, E. Pompei<sup>1</sup>, and W. Walsh<sup>4</sup>

<sup>1</sup> European Southern Observatory (ESO), Alonso de Cordova 3107, Santiago, Chile

<sup>2</sup> present address CEA, Service d'Astrophysique, 91191 Gif-sur-Yvette, France

<sup>3</sup> Osservatorio di Arcetri, Largo E. Fermi 5, 50125 Firenze, Italy

<sup>4</sup> Harvard Smithsonian Center for Astrophysics, 60 Garden St, MS 12, Cambridge, MA 02138, USA

Received 13 November 2001 / Accepted 19 February 2002

**Abstract.** We present observations in the optical, near-infrared and millimetre bands of the Ultraluminous Infrared galaxy IRAS 19254-7245, also known as “The Superantennae”. This galaxy is an interacting system with a double nucleus and long tails extending for about 350 kpc. We studied in detail the southern component of the system which is optically classified as a Sy2 galaxy. We have developed a method to determine the parameters of the emission lines in a spectrum in the case of multiple components and severe blending. Our data allow us to build a picture of the environment around the nucleus of the galaxy with unprecedented detail. The optical lines show a complex dynamical structure that is not observable in the near-infrared. In addition we find typical features of AGN such as the coronal lines of [FeVII]5721 and [SiVI]1.96. We also detect strong emission from [FeII]1.64 and H<sub>2</sub>.

**Key words.** galaxies: individual: IRAS 19254-7245 – infrared: galaxies – radio lines: galaxies – galaxies: Seyfert

## 1. Introduction

IRAS 19254-7245, with an infrared luminosity  $L_{\text{IR}} = 1.1 \times 10^{12} L_{\odot}$  (calculated assuming  $H_0 = 75 \text{ km s}^{-1} \text{ Mpc}^{-1}$ ,  $v = 18479 \text{ km s}^{-1}$  and using all four IRAS fluxes Melnick & Mirabel 1990), lies amongst the Ultraluminous Infrared Galaxies (ULIRGs) emitting most of their energy in the far infrared. More than 90% of these objects show evidence for disturbed morphologies and interaction (e.g. Sanders et al. 1988; Melnick & Mirabel 1990; Murphy et al. 1996; Clements et al. 1996). IRAS 19254-7245 is a particularly spectacular interacting galaxy with tidal tails extending to a distance of about 350 kpc and two bright nuclei 10 kpc apart. Although it is widely accepted that this system results from the collision between two gas-rich spirals, a multiple-merger origin has been recently suggested from high-resolution HST observations showing that a double nucleus may be present in both components of the interaction (Borne et al. 1999).

The southern nucleus prevails in luminosity as the system is observed at longer wavelengths and it is the dominant source in the mid-infrared as shown by the ISOCAM

observations of Charmandaris et al. (2002). This nucleus also shows an optical spectrum typical of a Seyfert 2 galaxy (Mirabel et al. 1991). The presence of strong nuclear activity is moreover indicated by the Near-Infrared (NIR) and IRAS 25/60<sup>1</sup> colors, which both suggest the presence of important thermal emission from hot dust ( $\sim 300\text{--}500 \text{ K}$ ) most probably heated by the active nucleus.

The system has been studied among others by Mirabel et al. (1991) and Colina et al. (1991). Both groups find broad emission lines in the optical with a complex profile that can be attributed to material falling onto the nucleus or to an outflow. The kinetic energy required to power such a flow may originate from stellar winds and/or supernovae. This strongly supports the picture of merger-driven starburst activity characterized by a high star formation rate ( $\sim 150 M_{\odot} \text{ yr}^{-1}$ , Colina et al. 1991), taking place in the Seyfert circumnuclear region.

Understanding the true origin of the ultra-luminous phase in infrared galaxies is still an open debate. Recent studies have shown that the merger-stage in interacting systems, traced by the projected separation of the nuclei, correlates with the star-forming efficiency and with the molecular mass detected in each merger (Gao & Solomon 1999; Murphy et al. 2001). However the relative importance between starbursting and AGN activity in luminous

Send offprint requests to: L. Vanz,

e-mail: lvanzi@eso.org

<sup>\*</sup> Based on observations obtained at the ESO telescopes of La Silla.

<sup>1</sup> Defined as  $\text{Log } f_{25}/f_{60}$ .

galaxies, and ULIRGs in particular, is still an open issue (Sanders & Mirabel 1996; Lutz et al. 1996; Vignati et al. 1999). Harboring both a Seyfert and a starburst components, IRAS 19254-7245 is a very interesting object within this context. The separation between the two nuclei involved in this merger is still large enough to allow a careful analysis and distinguish between the two sources. Our main goal is to study the near infrared (NIR) spectrum of this galaxy, but optical and *mm* data were also obtained.

The present paper is divided in three main sections: Observations, Analysis and Discussion. In Sect. 2 we present the data describing how they were obtained and reduced. In Sect. 3 we present the analysis of the data and how the main physical parameters were derived from the observations. In Sect. 4 we use these parameters to describe the physical conditions in the galaxy. Finally we summarize our conclusions.

## 2. Observations

### 2.1. Optical

We obtained low and medium resolution spectra of IRAS 19254-7245 at optical wavelengths. The low resolution spectrum was observed with the Boller & Chivens spectrograph at the ESO 1.52m telescope at La Silla in 1999 May using grating #23 and a 2''-wide slit to yield a spectral resolution of  $R = 1300$  in the range 4400–7400 Å. The position angle was  $-12^\circ$ , which allows to include both nuclei in the slit. The total integration time was 40 min. The 1D spectrum of the southern component extracted with an aperture of 2.6'' corresponding to 3.1 kpc at a distance of 247 Mpc, is shown in Fig. 1. The medium resolution spectrum was acquired with EMMI at the ESO-NTT in 1999 July using the REMD (Red Medium Dispersion) mode and grating #6 which gives a resolution  $R = 5500$  in the band 6600–7200 Å. Two exposures of 15 and 30 min were taken using a 1''-wide slit. HeAr lamp spectra were taken before and after the exposures for the wavelength calibration and the star EG 274 was observed as spectro-photometric standard. The spectra were reduced following standard procedures. The EMMI instrumental resolution, estimated on sky lines is  $36 \text{ km s}^{-1}$ . The flux calibration was obtained by comparing the wavelength calibrated spectra of the standard star with the flux table published. From the 2D combined frame we extracted 1D spectra with an aperture of 2.6''. A linear fit on the continuum gives a slight positive slope from  $9.4 \times 10^{-17}$  at 6600 Å to  $9.9 \times 10^{-17} \text{ s}^{-1} \text{ cm}^{-2} \text{ Å}^{-1}$  at 7200 Å. To double check the flux calibration we used a HST archive image taken in the F814W filter centered at 7940 Å. For our spectroscopic aperture we obtained a flux of  $1.09 \times 10^{-16} \text{ erg s}^{-1} \text{ cm}^{-2} \text{ Å}^{-1}$ , that agrees with our calibration to better than 5%. The medium resolution spectrum of the southern nucleus subtracted of the continuum is shown in the top panel of Figs. 2 and 3.

### 2.2. Near-infrared

We observed two spectra with the medium resolution grism of SOFI at the ESO-NTT. The spectra are respectively centered on the *H* and the *Ks* bands. They were acquired in 1999 May with 40 min of integration in *H* and 66 min in *Ks*. The *Ks* spectrum was observed again in 1999 September for 30 min of integration. We always used a 1''-wide slit giving a resolution  $R = 900$  in *H* and  $R = 1350$  in *Ks*. A low resolution spectrum ( $R = 600$ ) covering the range from 1.5 to 2.5  $\mu\text{m}$  has been obtained with SOFI in 2001 June, the total integration time was in this case 40 min. The position angle was always  $-12^\circ$ . The data reduction followed the standard steps for NIR spectroscopy. 1D spectra were extracted with an aperture of 2.6'' for the southern component. Atmospheric features were corrected by dividing for the spectrum of a reference star. In the observation of 1999 May we used a G1V and a F8V star, then the spectra were multiplied by the solar spectrum to remove the stellar features and reestablish the correct slope of the continuum (Maiolino et al. 1996). In 1999 September we used an O6 star and then multiplied by a blackbody at 40 000 K to reestablish the correct slope of the continuum. The *Ks* spectra observed on the two occasions give a good check on the reliability of this method; they are virtually identical showing no residual features from the reference star and exactly the same slope of the continuum. The *Ks* spectra have been averaged together giving a final spectrum with 1h 36m of integration. To flux calibrate the spectra we obtained two images in the *H* and *Ks* band with SOFI in 2001 June; the integration time was 15 min in each band. From the images we extracted the photometry on the spectroscopic aperture obtaining fluxes of  $3.16 \times 10^{-12}$  and  $2.80 \times 10^{-12} \text{ erg s}^{-1} \text{ cm}^{-2} \mu\text{m}^{-1}$  in *H* and *Ks* respectively. The photometric error was always below 3%. This value does not include the uncertainty on the spectroscopic apertures and on their centering, however we believe that this procedure guarantees a very accurate flux calibration. In the case of the low resolution spectrum the slope of the continuum was readjusted to match the photometric points. In Fig. 4 we present the NIR spectra of the southern nucleus. The top curve is the low resolution spectrum calibrated in flux. In the middle the medium resolution spectrum. In the bottom part of the left panel we show a stellar template redshifted to match the galaxy with the indication of the absorption features detectable. In the bottom right panel the *K* spectrum, with the  $\text{H}_2(1-0)\text{S}(3)$  line subtracted, clearly shows the detection of [SiVI] (see Sect. 3.2 for details). Our NIR spectra of the northern nucleus are virtually featureless.

### 2.3. Millimetre

The radio observations were performed with the Swedish ESO-Submillimetre Telescope (SEST) in La Silla during 1999 November. The *FWHM* beam sizes are 45'' and 23'' at 115 GHz and 230 GHz respectively, and the main beam efficiencies at these frequencies are 0.70 and 0.50. Intensity

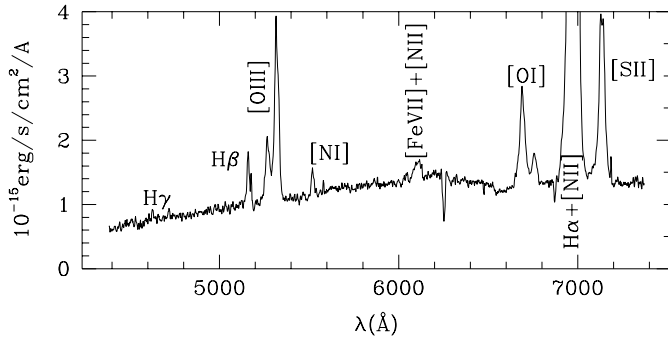


**Fig. 1.** Low resolution optical spectrum of IRAS 19254-7245 obtained at the 1.5 ESO telescope of La Silla.

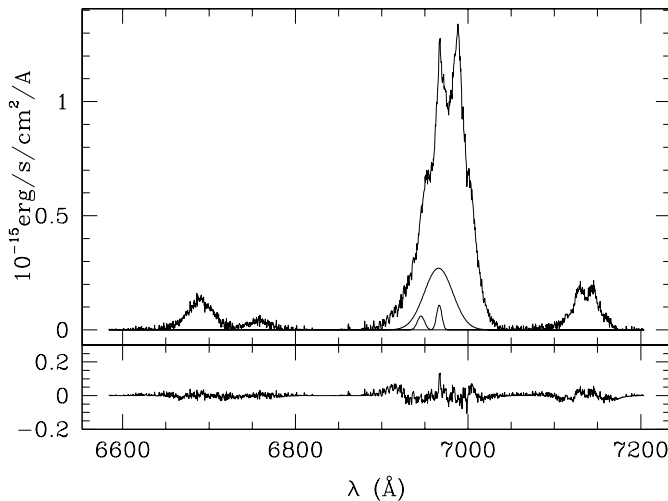


**Fig. 2.** Medium resolution optical spectrum of IRAS 19254-7245 observed with EMMI at the ESO-NTT. Top panel: the spectrum subtracted of the continuum and the three components of H $\alpha$  obtained with free  $\sigma$ . Bottom panel: the residuals of the fit.

calibration is done with the chopper wheel method, so the raw data, in units of  $T_*^A$ , are divided by the main beam efficiency to obtain main beam brightness temperatures. The internal consistency of the SEST is accurate to within a few percent.

The backends used were two acousto-optical spectrometers, each with a total bandwidth of 1 GHz. System temperatures ranged between 200 K and 350 K on the  $T_*^A$  scale. All observations of the CO lines were performed with  $\tau_{225 \text{ GHz}} \leq 0.4$ . The SEST's absolute pointing accuracy is  $3''$  rms in azimuth and elevation, and the pointing model was checked with regular observations of SiO maser sources. Beam switching mode was employed, where the secondary mirror was wobbled with a beam throw of  $697''$  in azimuth and scans obtained with reference positions on either side were coadded to ensure flat baselines. The data were reduced with the CLASS software of the Grenoble Astrophysical Group (GAG) package. A polynomial baseline of order one, or occasionally three, was removed from each spectrum before averaging. The spectra are shown in Fig. 4.

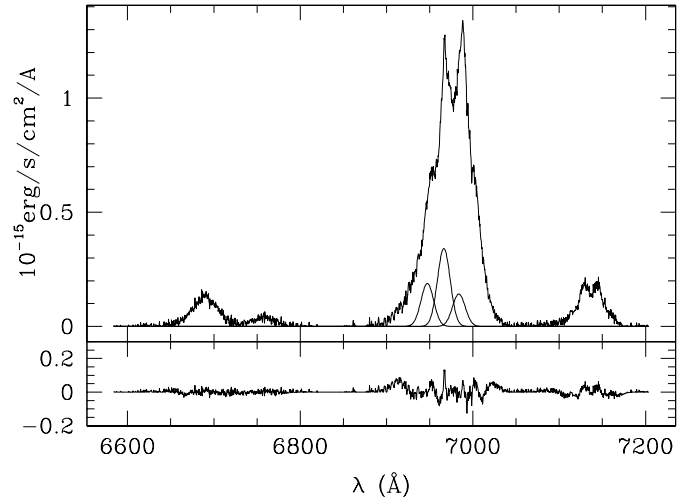


**Fig. 3.** Medium resolution optical spectrum of IRAS 19254-7245 observed with EMMI at the ESO-NTT. Top panel: the spectrum subtracted of the continuum and the three components of H $\alpha$  obtained with fixed  $\sigma$ . Bottom panel: the residuals of the fit.

### 3. Analysis

#### 3.1. The optical spectrum

The optical spectrum of the southern nucleus shows broad emission lines even at low resolution. At high resolution it is evident how each emission line contains more than one component. It is not an easy task to describe the lines in terms of simple components, since most of the lines in the observed spectral range observed are blended. After several unsatisfactory attempts with the most common data reduction packages we decided to develop our own code to produce the best fit of the observed spectrum taking into account all known constraints, mainly  $[\text{OI}]6363 = 0.33 [\text{OI}]6300$  and  $[\text{NII}]6583 = 3 [\text{NII}] 6584$ .

We considered three different cases: a 1-component model, a 2-component model and a 3-component model. For the 3-component model we have considered 2 cases, one with free  $\sigma$  for the lines, the other with fixed  $\sigma$ . The latter gives a more physical result given the type 2 nature of the Seyfert galaxy. We applied the inversion code to both the low resolution and the high resolution spectra. The best-fit parameters are given in Table 1, which is organized as follows.  $F_i$  denotes the fraction of the flux ascribed to the  $i$ th component of the line,  $z_i$  denotes the red-shift,  $\sigma_{\text{H}\alpha i}$  the standard deviation of the Gaussian of the  $i$ th component and refers to the H $\alpha$  line. It should be noted that the contribution due to the instrumental resolution,  $\sigma_{\text{instr}} \simeq 5 \text{ \AA}$  ( $FWHM$ ), and  $1.1 \text{ \AA}$  ( $FWHM$ ), for the low and the high resolution spectrum, respectively, is negligible compared to the intrinsic width of each component. The remaining rows in the table give the line integrated flux, due to *all* components of the various emission lines, in units of  $10^{-15} \text{ erg cm}^{-2} \text{ s}^{-1}$ . The residuals of the best fit to the high-resolution spectrum obtained assuming a 3-component model with free and fixed  $\sigma$  are shown in Figs. 2 and 3, along with the components of H $\alpha$ .

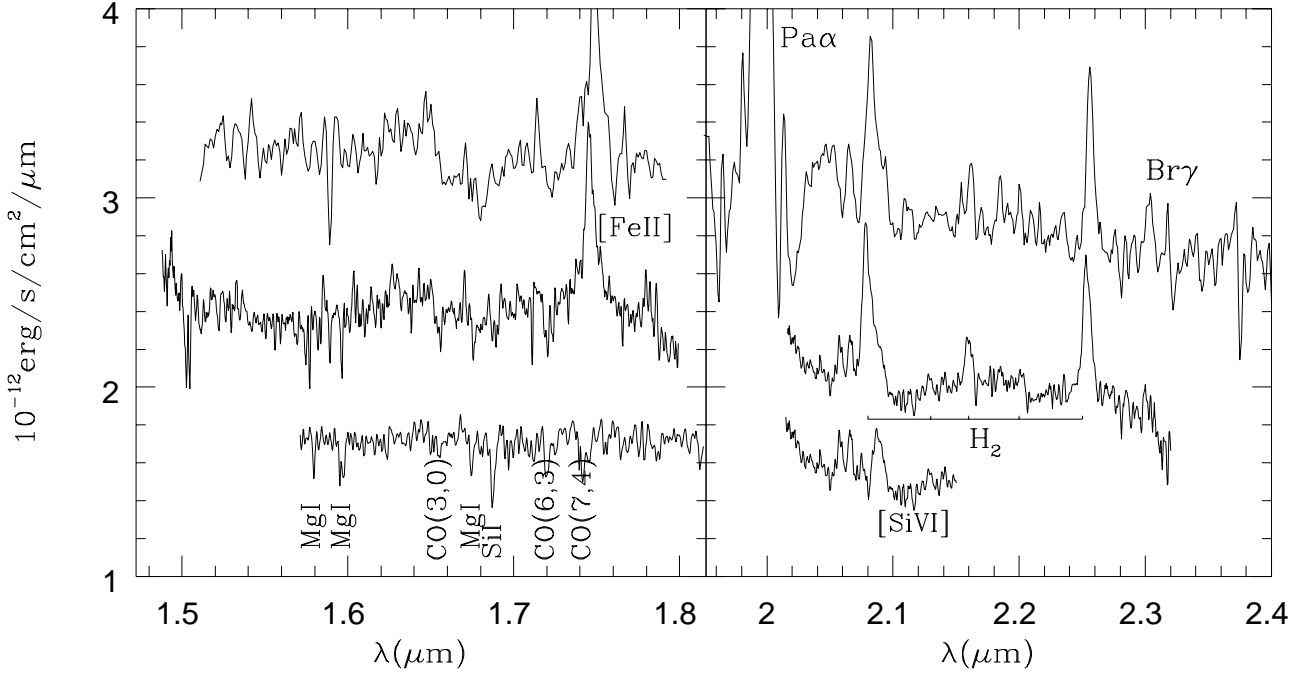


**Fig. 4.** NIR spectrum of IRAS 19254-7245 observed with SOFI at the ESO-NTT. From top low resolution, medium resolution, stellar template on the left and spectrum subtracted of the (1-0)S(3) line on the right. The flux scale only refers to the low resolution spectrum.

**Table 1.** Best-fit parameters for the 1, 2, and 3 component models. Fluxes are in units of  $10^{-15}$  erg cm $^{-2}$  s $^{-1}$ . See text for details.

Parameter	Low Resolution				High Resolution			
	1-Comp. Model	2-Comp. Model	3-Comp. Model		1-Comp. Model	2-Comp. Model	3-Comp. Model	
$F_1$	100%	88%	82%	55.0%	100%	91%	88.5%	51.0%
$F_2$		12%	12%	22.0%		9%	5.0%	28.0%
$F_3$			6%	23.0%			6.5%	21.0%
$z_1$	1.06153	1.06165	1.06196	1.06148	1.06132	1.06144	1.06141	1.06149
$z_2$		1.06148	1.06146	1.05850		1.06164	1.05831	1.05858
$z_3$			1.05422	1.06415			1.06153	1.06414
$\sigma_{H\alpha 1}$	21.1 Å	24.4 Å	22.0 Å	10.4 Å	22.2 Å	23.7 Å	23.3 Å	10.4 Å
$\sigma_{H\alpha 2}$		5.7 Å	5.6 Å	10.4 Å		4.7 Å	5.8 Å	10.4 Å
$\sigma_{H\alpha 3}$			12.6 Å	10.4 Å			4.3 Å	10.4 Å
H $\beta$	(4861 Å)	1.46	1.52	1.69	1.61			
O III	(4959 Å)	2.36	2.36	2.28	2.49			
O III	(5007 Å)	7.10	7.24	7.58	7.19			
N I	(5198 Å)	0.61	0.63	0.80	0.75			
Fe VII	(5721 Å)	0.26	0.27	0.10	0.10			
N II	(5755 Å)	1.06	1.05	0.87	0.87			
O I	(6300.3 Å)	3.59	3.77	4.63	4.09	3.70	3.89	3.43
S III	(6312.1 Å)	0.89	0.78	0.77	1.24	1.37	1.15	1.57
O I	(6363.8 Å)	1.18	1.24	1.53	1.35	1.22	1.28	1.14
Fe X	(6375.0 Å)			0.25	0.38			0.27
N II	(6548.1 Å)	10.94	10.49	10.03	11.01	12.8	12.1	13.47
H $\alpha$	(6562.8 Å)	19.35	22.0	25.28	18.75	13.7	17.1	12.59
N II	(6583.4 Å)	32.82	31.5	30.09	33.03	38.4	36.3	40.42
S II	(6716.4 Å)	7.01	7.15	7.76	6.57	3.38	4.05	3.12
S II	(6730.8 Å)	3.39	3.43	2.79	3.58	5.16	4.56	4.10

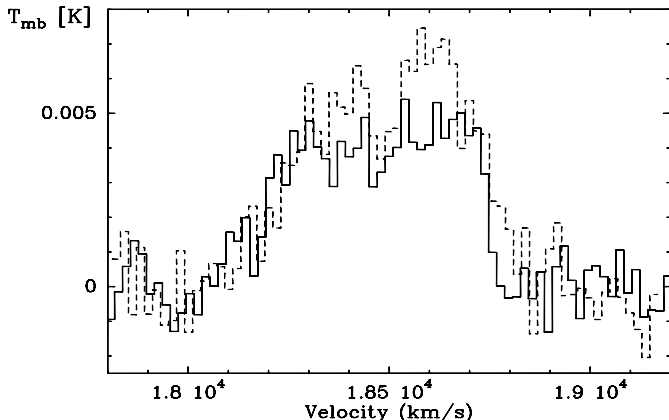


**Fig. 5.** SEST  $^{12}\text{CO}(1-0)$  (solid line) and  $^{12}\text{CO}(2-1)$  (dotted line) spectra of IRAS 19254-7245. The data have been smoothed to a velocity resolution of  $20 \text{ km s}^{-1}$ .

**Table 2.** NIR emission lines fluxes measured in  $10^{-15} \text{ erg s}^{-1} \text{ cm}^{-2}$ . (\*) have been measured in the low resolution spectrum only. The error on  $\text{P}\alpha$  is undetermined due to the bad atmospheric transmission.

line	$\lambda_{\text{obs}}$	$\lambda_{\text{rest}}$	Flux	$FWHM$ ( $\text{km s}^{-1}$ )
[FeII]	1.746	1.644	$5.9 \pm 0.1$	1200
$\text{P}\alpha$ (*)	1.993	1.875	$38 \pm ?$	630
Br 8	2.067	1.945	$1.0 \pm 0.3$	400
[SiVI]	2.087	1.962	$2.2 \pm 0.3$	1180
$\text{Br}\gamma$ (*)	2.300	2.165	$2.0 \pm 0.5$	-
<b>H<sub>2</sub> line</b>				
(1-0)S(3)	2.079	1.957	$5.8 \pm 0.2$	1070
(2-1)S(4)	2.129	2.003	$0.4 \pm 0.2$	-
(1-0)S(2)	2.160	2.034	$1.6 \pm 0.2$	765
(2-1)S(3)	2.200	2.070	$0.3 \pm 0.2$	-
(1-0)S(1)	2.254	2.121	$5.2 \pm 0.2$	880

The single component model is clearly insufficient to explain the observations. A much more satisfactory fit was obtained by assuming a 2-component model. The best results were obtained by assuming a 3-component model, and even better results would be expected by adding a fourth component (as done by Colina et al. 1991). However, increasing the number of free parameters leads to multiple solutions with similar values of the minimum  $\chi^2$ , which makes it virtually impossible to determine the most reliable one. The scattering between the various values obtained from the different models allows us to give the most appropriate estimate of the errors associated with the parameters, i.e., typically 3% for the high resolution spectrum.

### 3.2. The NIR spectrum

The NIR spectrum has a resolution that is significantly lower than the optical medium resolution spectrum and not enough to discriminate the various velocity components. For this reason it has not been necessary to apply

our code to the NIR part of the spectrum and all lines have been fitted with a single Gaussian component.

The [SiVI] line blended with the line (1-0)S(2) of  $\text{H}_2$  is clearly detected. To make this detection more evident and to measure the flux emitted we have subtracted from the (1-0)S(2) the profile derived from the (1-0)S(1) line. The best subtraction is obtained assuming a line ratio  $\text{S}(2)/\text{S}(1) = 1.17$ . The subtracted spectrum is shown in the bottom part of Fig. 4; the two faint lines on the left of [SiVI] can be identified with the residual of the OH 8-6 P1(4.5) sky line (Rousselot et al. 2000) and with  $\text{Br}\delta$ . In Table 2 the lines detected in the NIR spectrum and their fluxes are listed.

### 3.3. CO spectrum

Figure 5 shows the SEST spectra of the  $^{12}\text{CO}(1-0)$  and  $^{12}\text{CO}(2-1)$  emission in IRAS 19254-7245. The spectra have somewhat higher signal to noise than the  $^{12}\text{CO}(1-0)$  spectrum of Mirabel et al. (1991), as our SEST spectra have rms  $\sim 1.0 \text{ mK}$  when averaged to  $20 \text{ km s}^{-1}$  channels. Integrating these spectra we find a total  $^{12}\text{CO}(1-0)$  flux of  $I(\text{CO}) = 2.4 \pm 0.1 \text{ K km s}^{-1}$  and for  $^{12}\text{CO}(2-1)$   $I(\text{CO}) = 3.0 \pm 0.1 \text{ K km s}^{-1}$ , where the uncertainties are estimated following Elfhag et al. (1996). At the  $\Delta v_{20}$  level (width of the line at 20% of its peak value), the line widths are  $670 \pm 20 \text{ km s}^{-1}$  although there is a suggestion that the  $^{12}\text{CO}(2-1)$  spectrum is as wide as the  $800 \text{ km s}^{-1}$  claimed by Mirabel et al. (1991). The width at 50% level is  $570 \text{ km s}^{-1}$ . Both lines have a central velocity consistent with the heliocentric radial velocity of  $18500 \pm 80 \text{ km s}^{-1}$  generally adopted for IRAS 19254-7245. The differing beam sizes make line ratio considerations impractical with the current data.

## 4. Discussion

### 4.1. Extinction

From the ratio of the hydrogen recombination lines it is possible to calculate the extinction of the galaxy. Colina et al. (1991) derive  $E(B-V) = 1.40$  from the ratio of  $\text{H}\alpha$  and  $\text{H}\beta$  that corresponds to  $A_V = 4.37$  assuming the extinction curve of Rieke & Lebofsky (1985). Using 3 components to deconvolve the  $\text{H}\alpha$  at high resolution (see right column in Table 3) and the  $\text{H}\beta$  flux as measured at low resolution we obtain  $A_V = 3.15$ . We ascribe the difference with the value of Colina et al. to our better deconvolution of the spectrum. For the theoretical ratio of the two lines we have used the value 2.86 given by Osterbrook (1989) for  $T = 10^4 \text{ K}$  and  $n_e = 10^2 \text{ cm}^{-3}$ . An independent measure can be derived from the ratio  $\text{H}\beta/\text{Br}\gamma$ . Using the theoretical ratios 36.9 we obtain  $A_V = 3.9 \pm 0.2$ . This value, though less affected by the blending of the lines, has a much larger error. We do not use the  $\text{P}\alpha$  line that, though much brighter than  $\text{Br}\gamma$ , lies in a region of poor atmospheric transmission and cannot be considered reliable as evident from the high underlying noise visible in Fig. 4.

#### 4.2. Continuum

The four photometric points available for our spectroscopic aperture, mainly  $V$ ,  $I$ ,  $H$  and  $K$ s, give a rising continuum from the optical to the  $H$  band that significantly flattens toward the  $K$ s band. We tried to reproduce the global shape of the continuum using a simple model including cold stars, warm dust and a non-thermal continuum. The wide spectral range considered allows to put tight constraints despite the relatively small number of measured points. For our simplified model, each of these components was described by a black body at 3000 K, a black body at 1500 K and a power law with spectral index  $-0.5$ . A good fit was obtained with a 56% contribution from cold stars obscured by 4 mag of visual extinction, 28% from dust with 4 mag of extinction and 16% from the power-law. The latter, nonthermal component is required to flatten the NIR part of the spectrum; the same effect can however be obtained using a few hot stars heavily obscured or a cold star component with no extinction.

The NIR continuum of IRAS 19254-7245 appears rich of stellar absorption features most of which are CO bands. We compared our  $H$ -band spectrum with the spectrum of a stellar template obtained combining the spectra of late type stars (see Engelbracht et al. 1998), the result is shown in the bottom part of Fig. 4. We run a  $\chi^2$  test adding to the stellar template an increasing percentage of flat featureless continuum to measure the degree of dilution. We found a minimum for the  $\chi^2$  with a dilution by about 30%. Though this estimate is quite uncertain due to the moderate  $S/N$  and resolution, it is certainly indicative of the presence of some dilution of the continuum in the  $H$  band and it is not too far from the previous estimate. The absorption bands detected in the  $K$  band are too shallow to extend this kind of analysis to this band.

The discrepancy in the contribution of the cold star component derived with the two methods can be attributed to our over simplified model of the continuum and to the poor detection of the stellar absorption bands. We conclude that a significant fraction of the continuum originates from a hot dust component, probably close to the sublimation temperature, in the vicinity or within the torus of the AGN. This is consistent with the fact that a high fraction of the bolometric luminosity of the SuperAntennae originates from the nucleus of the southern galaxy as seen in the Mid-Infrared (Charmandaris et al. 2002).

#### 4.3. Line profiles

As already noted, the optical emission lines show a complex structure that cannot be reproduced by a simple Gaussian fit. From the analysis described in the previous section we have been able to obtain a satisfactory fit describing each line as the superposition of two or three components. The observed profiles can be explained by the presence of material that falls on or is ejected from

the nucleus, with typical velocities of about  $1000 \text{ km s}^{-1}$ , as shown by the parameters of the fit shown in Table 1.

On a larger scale, we have measured the rotation curve of the galaxy from the  $H\alpha$  2D spectrum. The curve is plotted in Fig. 6 with the southern nucleus at position 0. In this scale the northern component appears to be located at about 6 arcsec. The positions of both nuclei are marked by arrows. In the same figure we also plot the values of the velocity dispersion ( $\sigma$ ) deconvolved for the instrumental profile. The rotation curve is consistent with that measured by Mirabel et al. (1991); however our spatial resolution is higher. At position between 8 and 9 arcsec we detect a cloud of gas with a velocity of at least  $50 \text{ km s}^{-1}$  out of the main stream and a velocity dispersion lower than the average. This finding indicates that a dynamically complex structure is present even at large radial distances. The higher errors in the velocity and the higher values of dispersion around position 0 are mainly due to the complexity of the emission lines in this region. All lines observed in the optical are “narrow” in agreement with the classification of the south component as type 2.

It is interesting to note that the NIR lines do not show the complex profiles detected in the optical and that they can be well fitted by single Gaussians. This is possibly due to the lower resolution and lower  $S/N$  in the NIR that do not allow a good detection of the faint components. The velocity dispersion of the NIR lines are comparable to those in the optical indicating that the optical and NIR lines are probably generated in clouds that participate in the same motions. It would be interesting to compare the redshift of the NIR lines with the optical deblended lines but this would require a spectral resolution and wavelength accuracy higher than we have at the moment.

#### 4.4. Coronal lines

Two high ionization lines are detected in our spectra [FeVII]5721 and [SiVI]1.962. Both are blended with other lines and a careful de-blending process was used to measure a reliable value of the flux emitted. Marconi et al. (1994) proved that the ratio [FeVII]5721/[SiVI]1.962 is very close to unity in case of photoionization, independently of the details of the models. Correcting the fluxes measured in these lines for  $A_V = 4$  with the extinction law of Rieke & Lebofsky (1985) we obtain [SiVI]/[FeVII] = 0.5. This value however is quite uncertain due to the large uncertainty on the flux of the blended [FeVII]. In addition the low resolution optical spectrum was observed with a larger slit than the NIR one,  $2''$  instead of  $1''$ , and the [FeVII] could be diluted by the continuum. Although we have included the [FeX] line in our fit of the optical spectrum there is no direct evidence for the detection of this line.

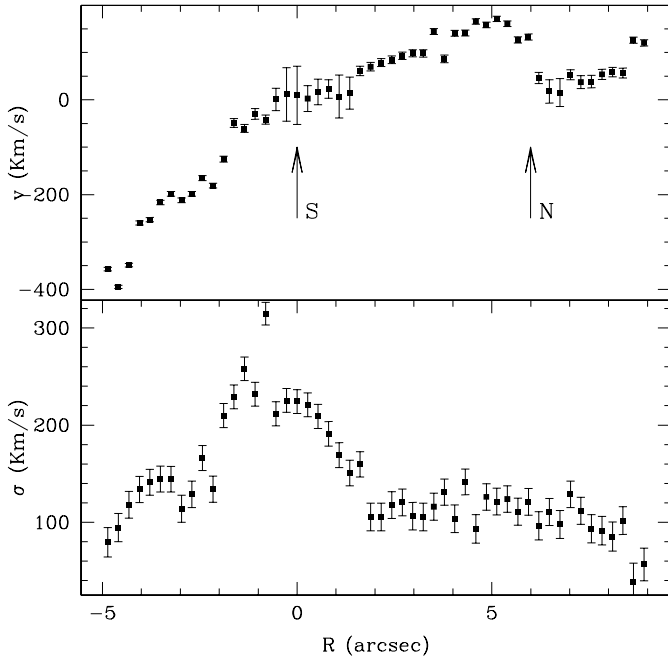


**Fig. 6.** Rotation curve (upper panel) and velocity dispersion (lower panel) of IRAS 19254-7245. The velocity is measured with respect to the southern component, the positions of the two nuclei are marked

#### 4.5. Lines of $H_2$ and $[FeII]$

We observe a very good NIR emission line spectrum from molecular hydrogen. In Table 3 we compare the observed ratios with the values predicted by two different models for fluorescent and thermal excitation derived from Engelbracht et al. (1998). From these ratios and from the non-detection of the  $H_2$  lines in the H spectrum we can assume to have a pure thermally excited spectrum. Two mechanisms can concur: shocks by either supernovae or nuclear jets and X-ray heating. The high ratio  $(1, 0)S(3)/(1, 0)S(1)$  would favor the second possibility at least according to the results from Mouri (1994). The same result would be inferred from the weakness of the  $(2-1)S(3)$  line according to Draine & Woods (1990). In Fig.7 we plot the excitation diagram of  $H_2$  as derived from our observations and built following Lester et al. (1988). From the diagram we can infer an excitation temperature of about 2000 K. The high excitation temperature allows us to exclude thermal excitation in photodissociation regions and favor the thermal process either by SN driven shocks or X-ray heating. The  $(1, 0)S(1)/Br\gamma$  ratio of 5.7 is unusually high even for a Seyfert galaxy (Moorwood & Oliva 1988). This makes IRAS 19254-7245 somehow similar to NGC 6240, however, unlike NGC 6240, the  $H_2$  emission is concentrated on the nucleus of the southern component and we detect no emission either from the northern nucleus or from the internuclear region. Though we cannot rule out that the interaction generates large shocks at least in the south galaxy, there is no direct evidence that could support the presence of such phenomena. Also the  $(1, 0)S(1)$  luminosity of about  $1.8 \times 10^7 L_\odot$  makes

of IRAS 19245-7245 a scaled down version of NGC 6240 ( $10^8 L_\odot$ ).

Very similarly to  $H_2$ , the ratio  $[FeII]/Br\gamma = 5.5$  is unusually high and again one of the highest after NGC 6240 in the list of galaxies observed by Moorwood & Oliva (1988); a similarly high ratio is reported by Vanzi et al. (1997) for the Seyfert 2 galaxy Arp 182. Such a high ratio is clear evidence for AGN, in fact values around one are expected in starbursting and HII galaxies while values above one are typical of AGNs. We can use the ratio  $[OI]/H\alpha = 0.17$  to locate the galaxy in a diagnostic diagram as the one of Alonso-Herrero et al. (1997). In such a plot IRAS 19254-7245 clearly seats in the Seyfert galaxies region. These high ratios are possibly due to the concurrence of excitation mechanisms such as shocks from SNE, AGN driven shocks and X-ray heating.

#### 4.6. Molecular hydrogen mass

The conversion of integrated line intensity of CO to surface mass density of molecular hydrogen involves making several assumptions (see Morris & Rickard 1982; Arimoto et al. 1996; Bryant & Scoville 1996; Sakamoto 1996; Verter & Hodge 1995; Hollenbach & Tielens 1997).

The conversion factor is currently the subject of much discussion, so for consistency many authors assume the commonly applied “standard Galactic” value of  $2.3 \times 10^{20} \text{ cm}^{-2} (\text{K km s}^{-1})^{-1}$  (Strong et al. 1988), although this value probably overestimates the true  $H_2$  mass in active galaxies. The “standard” value can be compared with independently estimated values from EGRET of  $1.56 \times 10^{20} \text{ cm}^{-2} (\text{K km s}^{-1})^{-1}$  (Hunter et al. 1997). Using our SEST flux with the relation for the conversion of CO line intensity into  $H_2$  column density given by Strong et al. (1988), and an adopted distance of 247 Mpc, we calculate an *indicative* estimate of the total molecular mass of  $M_{H_2} = 1.9 \times 10^{10} M_\odot$  that is consistent with a similar analysis presented by Mirabel et al. (1991), but should be regarded as an upper limit. Indeed, this molecular gas mass is about an order of magnitude higher than in typical spiral galaxies (Boselli et al. 1997; Casoli et al. 1998) and is somewhat larger than largest molecular gas mass ( $1.4 \times 10^{10} M_\odot$ ) found for a sample of interacting galaxies studied by Horellou & Booth (1997).

## 5. Conclusions

We have observed the Ultra Luminous Infrared Galaxy IRAS 19254-7245, concentrating our investigation on the southern component with observations that range from the optical to the millimetre. The results of our investigation can be briefly summarized as follow:

1. Based on our NIR and optical data we estimate a visual extinction between 3 and 4 mag. The continuum can be well reproduced assuming this value.
2. The optical emission lines have broad and complex profiles indicative of gas clouds rapidly moving around the

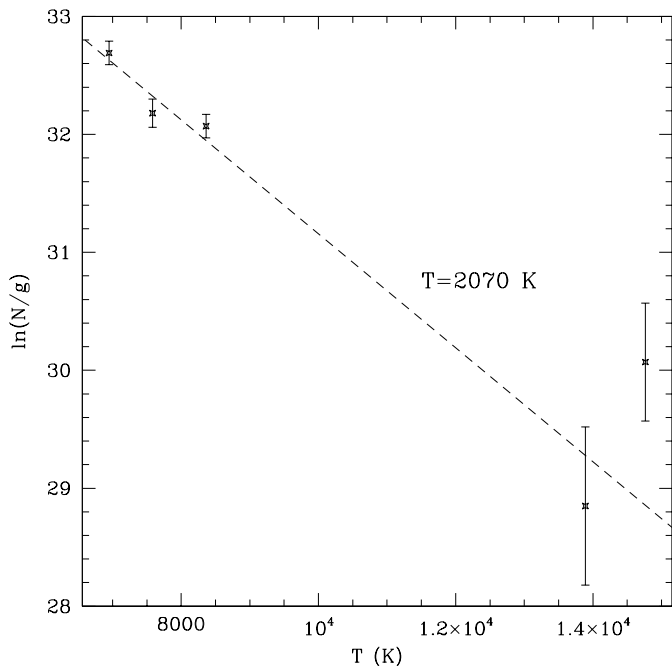


**Fig. 7.** Excitation diagram of molecular hydrogen in IRAS 19254-7245.

**Table 3.** Molecular hydrogen ratios.

line	observed	<i>fl</i>	<i>th</i>
(1, 0)S(3)	$1.13 \pm 0.23$	0.67	1.02
(2, 1)S(4)	$0.08 \pm 0.08$	0.12	0.02
(1, 0)S(2)	$0.35 \pm 0.12$	0.50	0.38
(2, 1)S(3)	$0.08 \pm 0.08$	0.35	0.08
(1, 0)S(1)	1.00	1.00	1.00

nucleus. The NIR lines are similarly broad though with a much simpler profile.

3. Coronal lines from [FeVII]5721 and [SiVI]1.96 are detected. Their ratio is consistent, within the error, with the value expected from photoionization.
4. NIR lines from H<sub>2</sub> and [FeII] are bright and give unusually high ratios with *B $\gamma$*  even for the AGN standards. The H<sub>2</sub> is thermally excited and has a very high luminosity ( $1.8 \times 10^7 L_{\odot}$ ).
5. From the CO luminosity we derive a H<sub>2</sub> mass of  $1.9 \times 10^{10} M_{\odot}$ .

*Acknowledgements.* We are grateful to Pierre-Alain Duc for making his NIR images of IRAS19254-7245 available to us and to Chad Engelbracht for sending to us his stellar template spectra. We also thanks Leonardo Testi for useful discussions and for his careful reading of the first draft of this paper. RM and ELF acknowledge the support of ESO under the visiting scientist and studentship programs respectively. We finally thank the anonymous referee for very useful comments that improved the present paper a lot.

## References

- Alonso-Herrero, A., Rieke, M. J., Rieke, G. H., & Ruiz, M. 1997, *ApJ*, 482, 747
- Arimoto, N., Sofue, Y., & Tsujimoto, T. 1996, *PASJ*, 48, 275
- Borne, K. D., Bushouse, H., Colina, A., et al. 1999, *Ap&SS*, 266, 137
- Boselli, A., Gavazzi, G., Lequeux, J., et al. 1997, *A&A*, 327, 522
- Bryant, P. M., & Scoville, N. Z. 1996, *ApJ*, 457, 678
- Chatzichristou, E. T. 2000, *ApJS*, 131, 71
- Casoli, F., Sauty, S., Gerin, M., et al. 1998, *A&A*, 331, 451
- Charmandaris, V., Laurent, O., & Le Floch 2002, *A&A*, submitted
- Clements, D. L., Sutherland, W. J., McMahon, R. G., & Saunders, W. 1996, *MNRAS*, 279, 477
- Colina, L., Lipari, S., & Macchetto, F. 1991, *ApJ*, 379, 113
- Draine, B. T., & Woods, D. T. 1990, *ApJ*, 363, 464
- Duc, P. A., Mirabel, I. F., & Maza, J. 1997, *A&AS*, 124, 533
- Elfhag, T., Booth, R. S., Hoeglund, B., Johansson, L. E. B., & Sandqvist, A. 1996, *A&AS*, 115, 439
- Engelbracht, C. W., Rieke, M. J., Rieke, G. H., Kelly, D. M., & Achtermann, J. M. 1998, *ApJ*, 505, 639
- Gao, Y., & Solomon, P. M. 1999, *ApJ*, 512, L99
- Hollenbach, D. J., & Tielens, A. G. G. M. 1997, *ARA&A*, 35, 179
- Horellou, C., & Booth, R. 1997, *A&AS*, 126, 3
- Hunter, S. D., Bertsch, D. L., Catelli, J. R., et al. 1997, *ApJ*, 481, 205
- Lester, D. F., Harvey, P. M., & Carr, J. 1988, *ApJ*, 329, 641
- Lutz, D., Genzel, R., Sternberg, A., et al. 1996, *A&A*, 315, L137
- Maiolino, R., Rieke, G. H., & Rieke, M. J. 1996, *AJ*, 111, 537
- Marconi, A., Moorwood, A. F. M., Salvati, M., & Oliva, E. 1994, *A&A*, 291, 18
- Melnick, J., & Mirabel, F. 1990, *A&A*, 231, L19
- Mirabel, I. F., Lutz, D., & Maza, J. 1991, *A&A*, 243, 367
- Moorwood, A. F. M., & Oliva, E. 1988, *A&A*, 203, 278
- Morris, M., & Rickard, L. J. 1982, *ARA&A*, 20, 517
- Mouri, H. 1994, *ApJ*, 427, 777
- Murphy, T. W., Armus, L. Jr., Matthews, K., et al. 1996, *AJ*, 111, 1025
- Murphy, T. W., Soifer, B. T., Matthews, K., & Armus, L. 2001, *ApJ*, in press [[astro-ph/0103425](#)]
- Osterbrock, D. E. 1989, *Astrophysics of Gaseous Nebulae and Active Galactic Nuclei*, University Science Books
- Rieke, G. H., & Lebofsky, M. J. 1985, *ApJ*, 288, 618
- Rousselot, P., Lidman, C., Cuby, J. G., Moreels, G., & Monnet, G. 2000, *A&A*, 354, 1134
- Sakamoto, S. 1996, *ApJ*, 462, 215
- Sanders, D. B., Soifer, B. T., Elias, J. H., et al. 1988, *ApJ*, 325, 74
- Sanders, D. B., & Mirabel, I. F. 1996, *ARA&A*, 34, 749
- Strong, A. W., Bloemen, J. B. G. M., Dame, T. M., et al. 1988, *A&A*, 207, 1
- Vanzì, L., Alonso-Herrero, A., & Rieke, G. H. 1998, *ApJ*, 504, 93
- Vignati, P., Molendi, S., Matt, G., et al. 1999, *A&A*, 349, L57
- Verter, F., & Hodge, P. 1995, *ApJ*, 446, 616
- Wolfire, M., Hollenbach, D. J., & Tielens, A. G. G. M. 1993, *ApJ*, 402, 195